JOURNAL OF MARINE ENGINEERING & TECHNOLOGY
https://doi.org/10.1080/20464177.2023.2281742

Taylor & Francis
Taylor & Francis Group

Autonomous docking of a feeder vessel

Bas J. de Kruif

MARIN, Maritime Research Institute Netherlands, Wageningen, Netherlands

ABSTRACT

Autonomous sailing is seen as one of the possible solutions to cope with the decrease in qualified personnel and to minimise the risk to humans and ships in challenging conditions. Autonomy is not limited to sailing a vessel safely through the seas, but it also includes docking the vessel. A feeder vessel distributes cargo and spends a relative large percentage of its time on (un)docking. Automating this part of the operation is expected to help save on resources. The objective of this work is to automatically approach a dock with an underactuated vessel. It comprises of both the design of a time-dependent trajectory, and a controller that can track this trajectory. The solution is tailored for our 71 m long feeder vessel designed for the eu-h2020 Moses project. The focus is on approaching the dock from cruising speed until the speed of the vessel is near-zero. The result of the study is a high-fidelity time simulation that shows the behaviour of the vessel in combination with the control system when it approaches a dock. The simulations show that the ship can approach the dock with coupled azimuthing thrusters to a speed when the bow thrusters become effective. The vessel then becomes fully actuated and can safely dock with its dynamical positioning system.

ARTICLE HISTORY
Received 4 April 2023
Accepted 4 November 2023

KEYWORDS
Automatic docking; maritime autonomous surface ship (MASS); Guidance-Navigation-Control; trajectory tracking

1. Introduction

Autonomous sailing is seen as one of the possible solutions to cope with the decrease in qualified personnel and to minimise the risk to humans and ships in challenging conditions. Autonomy is not limited to moving the vessel safely through the seas, but it also includes docking and undocking the vessel. Feeder vessels collect shipping containers from different ports and transport them to central container terminals where they are loaded to bigger vessels, or vice versa. Container ships with a capacity below 3000 TEU, with an average between 300 and 1000 TEU are typically called feeder vessels. Such vessels spend a relatively large percentage of their time on (un)docking compared to a seafaring cargo vessel. Automating this part of the operation, therefore, can save on resources.

The objective of this work is to automatically approach a dock. The focus is on approaching the dock from cruising speed to a near-zero speed, where the dynamical positioning system ought to take over for a fully autonomous docking operation. This is deemed the most critical part of the docking manoeuvre as the ship has to decelerate and steer without bow thrusters and hence is underactuated, that is, has less actuators than degrees of freedom. The study comprises the design of a time-dependent trajectory, as well as a controller that can track this trajectory. We aim to have the controller as simple as possible such that the parameters identification and tuning can be done in a planned experiment. The solution is tailored to our 71 m long feeder vessel designed for the EU-H2020 MOSES project (Moses 2023). The vessel has two azimuthing thrusters and two bow tunnel thrusters. A schematic representation of the ship used in this study is shown in Figure 1.

Approaches encountered in the literature to automatically dock a vessel can be broadly divided into Optimal Control Problem (OCP) approaches and Guidance-Navigation-Control (GNC) approaches. Initial work on OCPs calculated a (time-dependent) optimal trajectory and the accompanying actuator commands at the beginning of the run only (Djouani and Hamam 1995; Ohtsu et al. 1996). The pose of the ship had to be equal to the initial condition of the OCP for the actuator commands to be correct. However, this pose is only known during the actual sailing, and solving the OCP at that measured pose took too much time to use in real-time (Ahmed and Hasegawa 2015; Okazaki and Ohtsu 2008). A solution to circumvent this issue is pre-solving a set of OCPs with different initial conditions, and interpolating between them during the actual sailing. The OCP approaches were extended to obstacle avoidance in the harbour and/or to avoid collisions with other ships (Liu et al. 2020). With the increase of computational power, one does not need to interpolate between pre-calculated solutions from the beginning of the run; the OCP can be solved at the actual pose. This eventually leads to Model Predictive Control (MPC), where the OCP is not only solved at the start of the approaching phase, but it is solved at *every* time step (Martinsen et al. 2019; Li et al. 2020; Ravikumar et al. 2020). Finally, the optimal trajectory that results from the OCP can also be calculated at a low sampling frequency, and then tracked at a high sampling frequency with a vehicle controller. The vehicle controller can in its turn be a MPC (Mizuno et al. 2015), or another type of controller (Bitar et al. 2020; Martinsen et al. 2020).

GNC,on the other hand, splits the guidance and the vehicle control into two problems, where this is one combined problem in OCP. Guidance guides the path of a ship towards a given point, which in general may be moving (Shneydor 1998). The output of the guidance is hence a set of variables that the vehicle controller can track. This would generally be heading, or course, and speed for an underactuated ship. The guidance for automatic docking typically consist of a trajectory or path, either automatically generated or specified by a user, and a guidance law. The guidance law, such as Line-Of-Sight (LOS), Pure-Pursuit (PP), or Constant-Bearing (CB), is then used to provide setpoints to the vehicle controller such that it tracks this trajectory to the dock (Fossen 2021).

Tzeng et al. (2006) and Piao et al. (2019) provide a path manually by placing the final waypoint at a safe location near the docking loca-

CONTACT Bas J. de Kruif b.j.d.kruif@marin.nl

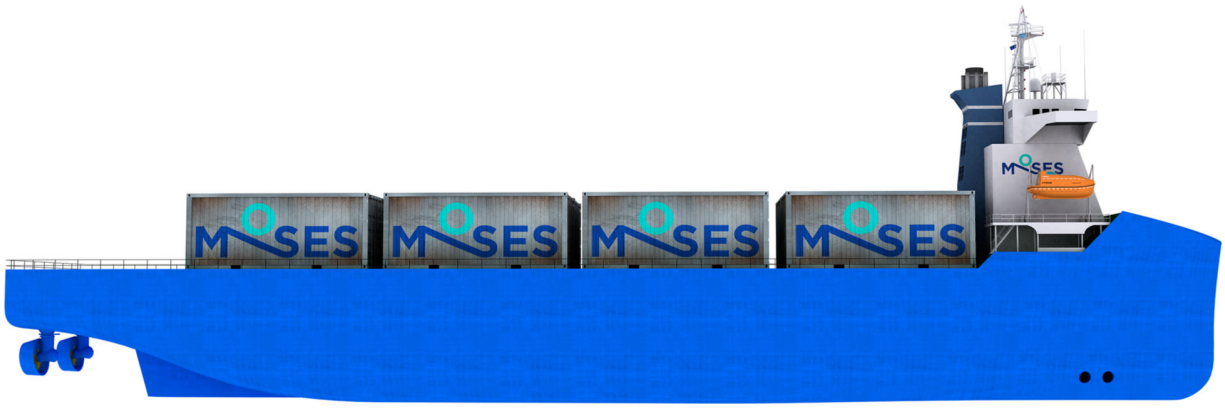

Figure 1. Feeder vessel used in this study.

tion where the ship should come to standstill. A LOS guidance law is used to steer the ship there. A smoother trajectory is obtained by Liao et al. (2019). They provide a path by specifying a set of waypoints on a Bézier curve that ends at the safe location near the dock. The velocity setpoint is a function of the distance to the docking location in these references. Next to placing the waypoints on a smooth curve, they can also be placed on a trajectory calculated from an OCP (Okazaki and Ohtsu 2008), or the curve itself can be used directly with a LOS guidance law (Sawada et al. 2021).

Both OCP and GNC approaches have been shown to give good results in literature. In the present work, the GNC approach is employed due to its simplicity of implementation and the low computational need. The split in functionality in GNC allows for future modification of a single element while retaining others.

For the design and evaluation of our docking solution we employ two different models. A simulation model is used to evaluate the performance of the controlled system. It is based on manoeuvring coefficients and is available in our in-house simulation environment. The manoeuvring coefficients were determined through CFD calculations. This simulation model is too complex to design a controller with, so a simplified control model is deduced from it. Both simulation and control model are treated in Section 2.

Guidance is treated in Section 3. First a trajectory is generated that provides the latitude and longitude in time. However, at cruising speeds the bow thrusters of the ship are not available and we cannot track all the degrees of freedom simultaneously. A Constant-Bearing guidance law is used to convert the trajectory setpoint to a required course and speed. This guidance law is selected as it not only uses the instantaneous position of the trajectory but also its velocity. The velocity is fed forward to the velocity required of the vessel and hence allows to track the target without a position error. An example usage of CB is when two ships sail next to each other in a replenish operation (Skejic et al. 2009). As shown in Fruzzetti et al. (2022), other guidance laws might be considered for tracking a target. Next to the setpoint for course and surge speed, all their derivatives can be provided by the guidance. This, in its turn, can be used to include our knowledge on ship motions in the feed forward part of the controller. The design of the controller is treated in Section 4. The designed controller is tested on the detailed simulation platform to evaluate its performance in Section 5. The results are elaborated upon in the same section. Conclusions are drawn in Section 6.

The main contribution of this paper is considered to be the combination of the analytic trajectory with the CB guidance law that also provides all the derivatives needed to use the ship knowledge in a feed forward controller. The accompanying feedback controller could then be designed with linear tools to stabilise the ship and reject disturbances and model uncertainty. The GNC could bring the ship to a near standstill at a safe pose close to the dock. This paper is an extended version of the work previously presented at the iSCSS 2022 conference (de Kruif 2022b).

2. Ship motion model

Two models are used in this study. First, a detailed numerical model that is available in our simulation environment (MARIN 2022). This model is used in all the simulations and is hence called the simulation model. Second, a simplified control model is used to design a controller on. It is deduced from the behaviour of the simulation model. This is equivalent to how a model would be obtained through system identification on a real vessel.

2.1. Simulation model

The simulation model is assumed to be given and is treated in an earlier publication (van Daalen et al. 2023). The elements included are:

- Hydrostatic forces that are calculated based on the 3D hull shape. There are linearised because we only have small roll and pitch angles.
- Hydrodynamic forces such as calm water resistance and manoeuvring forces. These are first simulated by means of CFD computations, and then approximated by a set manoueuvring coefficients for a time-domain simulation.
- Wave radiation forces that are included as frequency dependent mass and damping.
- Wave excitation of the vessel. This is calculated by linear radiation-diffraction theory. It results in first and second order wave loads.
- Four quadrant propeller characteristics for the azimuthing and bow thrusters are used to relate the force and torque generated based on their RPM.

The equations of motion are solved for all 6 degrees of freedom and contain coupling between them.

2.2. Control model

The velocity and course are considered decoupled for the *control* model in this work. It is assumed that both variables change sufficiently slow, and are individually controlled tightly enough. The velocity is considered a parameter in the course model. As long as

the drift angle is limited, this assumption will hold. If the (course unstable) ship will start to run out of its rudder, the velocity will drop quickly, and this assumption will no longer hold. The identification of the course model is done in two steps. First the rate-of-turn is identified as a result of lateral forces, and then the course is identified as a result of the rate-of-turn.

2.2.1. Rate-of-turn model

The ship used in this study is course unstable. This behaviour can be described by a first order Nomoto model (Neuffer and Owens 1991):

$$\dot{r} = -\frac{K}{T}(\alpha + \beta r^2)r + \frac{K}{T}F_y. \quad (1)$$

Here the rudder angle has been replaced by the lateral force F_y. In this equation r denotes the rate-of-turn, and $\alpha < 0, \beta > 0, K/T > 0$ are parameters to be determined. The values of α, β can be found by fitting them on a Bech's reverse spiral, while the value of K/T is found by the step response around the $F_y = 0$ N equilibrium.

The results of the identification simulations are shown in Figure 2. Figure 2(a) shows the relation between the rate-of-turn and the lateral force. Running the simulation for different fixed surge velocities results in a set of curves. The top of Figure 2(b) shows the fit of the Bech's reverse spiral for $u = 2.5$ m/s. The grey line is from the simulation, the orange line is the fit. The fitted parameter values of α, β are presented in Table 1. Note that both α and β are speed dependent.

The bottom part of Figure 2(b) shows the response to step changes on the lateral force at the equilibrium $F_y = 0$ N with a solid grey line. The dashed line shows the $1 - \exp(-1) = 63\%$ change from the minimum to the maximum amplitude from which the time constant of the first order system is deduced, which is directly related to K/T. When this time constant is used to estimate the response at $t = 1500$ seconds, then the orange line is found. For velocities below 1 m/s a first order model does not adequately describe the response.

The linearised transfer function of (1) for $r = 0$ rad/s is found as:

$$\frac{r}{F_y} = \frac{K/T}{s + \alpha K/T}. \quad (2)$$

s indicates the Laplace variable. The pole corresponding to the linearised system is given in Table 1 and the positive sign shows the unstable behaviour of the system at this operating point. The location of the pole changes to the left-half plane if we linearise around an increased rate-of-turn.

Table 1. Parameter values identified for the three parts of the control model.

Model	Parameter	Pole/zero
rate of turn	$\alpha = -8.47\,10^5 \cdot u$	$p_{r=0} = 9.27\,10^{-3} \cdot u$
	$\beta = 4.84\,10^9/u$	
	$K/T = 1.09\,10^{-8}$	
course	$a = 9.784\,10^{-3} \cdot u$	$p = -9.78\,10^{-3} \cdot u$
	$b = -0.512$	$z_1 = -7.62\,10^{-3} \cdot u$
	$c = -10.1/u$	$z_2 = 3.19\,10^{-2} \cdot u$
speed	$m - X_{\dot{u}} = 3.3\,10^6$	
	$X_{u\|u\|} = -1506$	

Note: The right-most column indicate the poles and zeros for the linearised transfer function.

2.2.2. Course model

The relation between the course and the rate-of-turn is based on the work of Yu et al. (2008):

$$\dot{\chi} = -a\chi + a\psi + (1+b)\dot{\psi} + c\ddot{\psi} \rightarrow \dot{\kappa} = -a\kappa + b\dot{\psi} + c\ddot{\psi}, \quad (3)$$

in which χ denotes the course, ψ the heading and $\kappa = \chi - \psi$ the slip angle. a, b, c are parameters. In the cited reference the parameter c is not present. However, if we apply a lateral force, the vessel will move to the side first, and only when it has rotated, then the surge speed will change the course to the other direction. At lower speeds, this effect is significant. This non-minimum phase behaviour is caught when $c \neq 0$, and is shown in Figure 3.

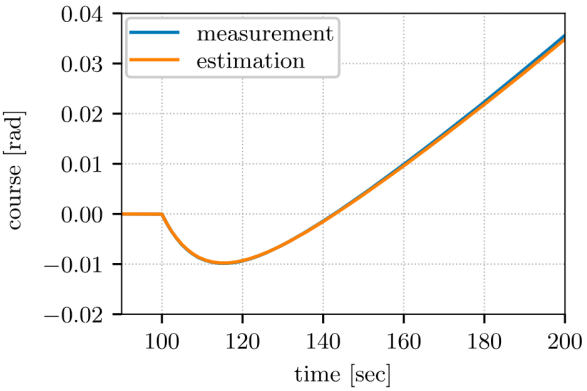

Figure 3. The course with fixed surge speed $u = 0.5$ m/s and a step on the reference rate-of-turn.

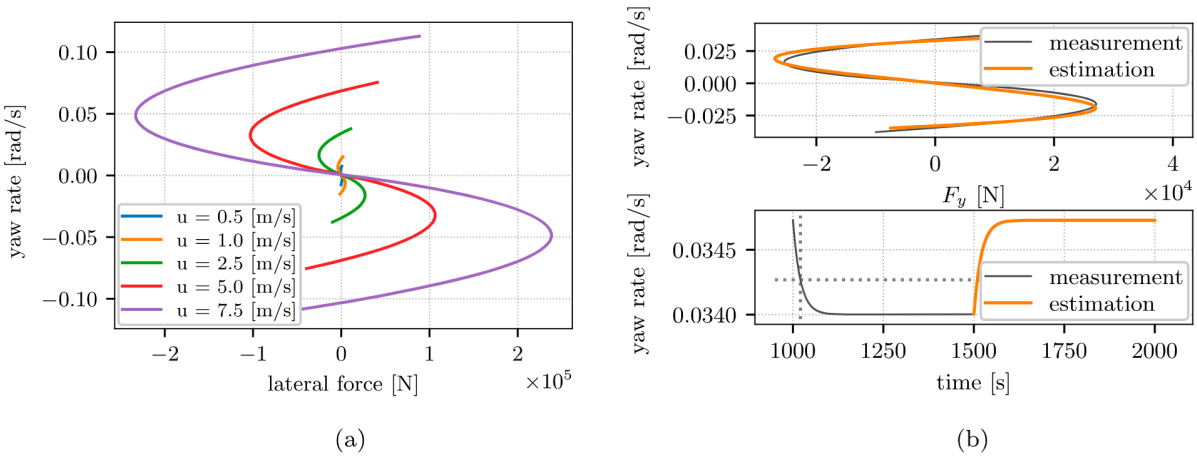

(a) (b)

Figure 2. Identification of the rate-of-turn model from a detailed numerical model. (a) Bech's reverse spiral test and (b) fit of the simulations at $u = 2.5$ m/s.

The parameters values were identified in a closed loop simulation in which the rate-of-turn was controlled. The rate-of-turn setpoint was changed stepwise. By means of a least squares fit the relation between the slip angle and rate-of-turn in (3) was calculated. The values are shown in Table 1. Figure 3 shows the course when the rate-of-turn reference value is changed at $t = 100$ sec. The non-minimum phase behaviour of the course due to the lateral force is clearly present at this low velocity. Figure 3 shows that the simulation and the approximation are nearly identical for this velocity. The transfer function of (3) is calculated as:

$$\frac{\chi}{r} = \frac{cs^2 + (1+b)s + a}{s(s+a)} = \frac{(\tau_{z_1}s+1)(\tau_{z_2}s+1)}{s(\tau_p s+1)} \tag{4}$$

in which we have used the knowledge that the transfer from heading to course is equal to one when sailing straight. The pole and zero locations are the inverses of the time constants τ. Their values are given in Table 1. The second zero is in the right-hand plane and it approaches the imaginary axis for low speed. This zero limits the bandwidth of a course controller.

2.2.3. Speed model

The manoeuvering model for the surge speed, with the hydrodynamic cross coupling removed, is given as:

$$(m - X_{\dot{u}})\dot{u} = mvr + X_{u|u|}u|u| + F_x, \tag{5}$$

where m gives the rigid body mass, $X_{\dot{u}}$ the added mass, $X_{u|u|}$ the quadratic damping, u, v, r are the velocities in surge, sway and yaw direction. F_x denotes the longitudinal force. The parameter values are again given in Table 1.

3. Guidance

3.1. Trajectory generation

An optimal path to approach a dock can be determined as OCP. However, solving an OCP can be computationally demanding and might be difficult in real-time applications. In de Kruif (2022a) it has been shown that Bézier curves can be used to generate smooth trajectories and their corresponding time derivatives. The acceleration and rate-of-turn values are limited when the trajectory is not too challenging, but must be checked afterwards. No limits on the actuators can be set beforehand.

Before the approach to the dock is started, the vessel is assumed to be sailing from waypoint to waypoint. When the ship is at a distance of around 13 ship lengths, which is slightly above 900 metres for our feeder vessel, the approaching phase is initiated. This distance is found to be a good distance to start the approaching phase of the operation: A larger distance would have the ship sail straight to this distance, after which the same trajectory results. If a shorter distance would be used, the total duration of the operation would take longer, or it would even become infeasible to dock at all (de Kruif 2022a).

At the initial position, a cubic Bézier curve is constructed that starts at this position, and ends at the required position close to the dock. Refer to Appendix 1 for additional information and symbols used. The initial and final position define the values for control points $\boldsymbol{p}_0$ and $\boldsymbol{p}_3$. The tangent at $\boldsymbol{p}_0$ is equal to the vector from $\boldsymbol{p}_0$ to $\boldsymbol{p}_1$ and is set to the initial course. The length of this vector is set to $l_0 = 0.6D$, which closely matches (Sawada et al. 2021), and fully specifies $\boldsymbol{p}_1$. D is the distance to the dock. The value for $\boldsymbol{p}_2$ is set such that the vector from it to $\boldsymbol{p}_3$ equals the final heading. Through a one-dimensional numerical optimisation the length of this vector is set to minimise the rate of turn.

The resulting Bézier curve is a path in space only, and is dependent on its path variable h. A relation between the path variable and time makes the path a time-dependent trajectory. If we relate the path variable to time as $h = \frac{tu_0}{6l_0}(2 - \frac{tu_0}{6l_0})$ in which t denotes time, and u_0 the initial velocity, see Figure A1, then we will decrease the velocity from u_0 to zero. An example trajectory is shown in Figure 4. The trajectory provides us with a target position $\boldsymbol{p}_t = [p_{t,x}, p_{t,y}]^T$ and velocity $\boldsymbol{v}_t = [v_{t,x}, v_{t,y}]^T$ in earth fixed coordinates.

3.2. Constant bearing guidance law

A CB guidance law is used to provide a setpoint to the vehicle controller such that the vessel will converge with the target, that is, the current point of the trajectory. In guidance texts, our own vessel is often referred to as interceptor. The setpoint velocity vector,

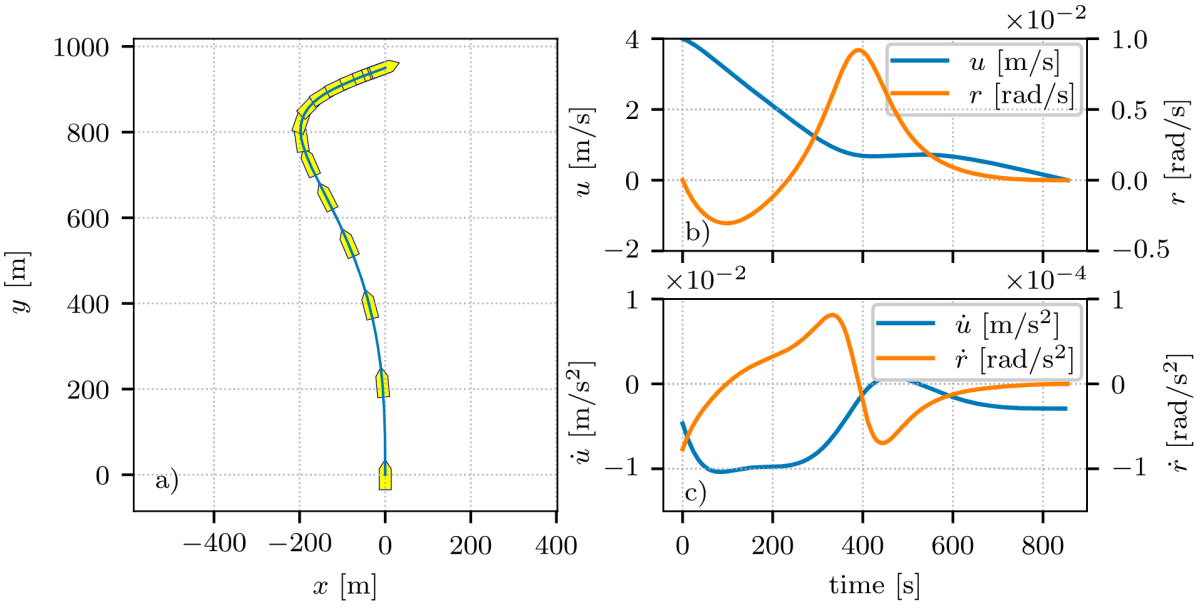

Figure 4. Generated Bézier trajectory. (a) shows the path, while (b), (c) show the velocities and accelerations for the surge velocity, u and rate of turn, r respectively.

$\boldsymbol{v}_{sp} = [v_{sp,x}, v_{sp,y}]^T$, for our vessel is given as Breivik (2010):

$$\boldsymbol{v}_{sp} = \boldsymbol{v}_t + \boldsymbol{v}_a = \boldsymbol{v}_t + \gamma \frac{\tilde{\boldsymbol{p}}}{||\tilde{\boldsymbol{p}}||} \quad \text{with } \tilde{\boldsymbol{p}} = \boldsymbol{p}_t - \boldsymbol{p}. \tag{6}$$

In this equation, the velocity setpoint is composed of the target velocity and a correction velocity, $\boldsymbol{v}_a$, that steers our vessel to the current position of the target. The velocity to the target has magnitude γ, and is in the direction of the difference of the target position $\boldsymbol{p}_t$ and our present position $\boldsymbol{p}$. The speed and course setpoints to the vehicle controller, u_{sp} and χ_{sp} are obtained from this:

$$u_{sp} = ||\boldsymbol{v}_{sp}||_2, \quad \chi_{sp} = \arctan_2(v_{sp,y}, v_{sp,x}). \tag{7}$$

The value of γ results from the distance between the target position and the actual vessel position:

$$\gamma = U_{max} \frac{\sqrt{\tilde{\boldsymbol{p}}^T \tilde{\boldsymbol{p}}}}{\sqrt{(\tilde{\boldsymbol{p}}^T \tilde{\boldsymbol{p}} + \Delta^2)}}. \tag{8}$$

The parameter U_{max} is the maximum speed by which our vessel is moving toward the target point, and Δ the distance at which U_{max} is halved. U_{max} should be smaller than the velocity at which the bow thrusters become effective and the fully actuated control system takes over to avoid sudden course changes. These sudden changes occur if the ship overtakes the target, and the correction velocity, $\boldsymbol{v}_a$ becomes larger than the target velocity $\boldsymbol{v}_t$. The course in (7) then changes quickly. This can be avoided by limiting U_{max}. However, setting U_{max} small makes the convergence slow. The value of Δ is increased until a smooth operation is obtained. The setpoints' time derivatives are provided in Appendix 2.

4. Control

The vehicle control calculates longitudinal and lateral forces such that the measured surge velocity and course match their setpoint as good as possible.

4.1. Course control

The controller to keep course is designed as a cascade controller. This approach is used so that the non-linearities and the unstable pole of the inner loop can be addressed first. The resulting inner loop then becomes stable, which allows for a simple outer-loop design. A single loop compensator with an unstable zero and pole would otherwise lead to a high sensitivity peak (Skogestad and Postlethwaite 2007). An overview of the cascade controller with the system model described in Section 2 is shown in Figure 5.

4.1.1. Rate-of-turn controller

The rate-of-turn controller consists of a feedback controller and a feed forward controller. The feed forward controller calculates the lateral force based on the set point for the rate-of-turn, while the feedback controller compensates for deviations. The feed forward signal can be calculated directly from (1):

$$C_{r,ff} : F_y = \alpha r_{sp} + \beta r_{sp}^3 + \frac{T}{K} \dot{r}_{sp}. \tag{9}$$

In this, and following equations, the subscript 'sp' indicates the set point value. The feedback controller is based on (2). When the loop is closed with:

$$C_{r,fb} : F_y = K_d(r_{sp} - r), \tag{10}$$

we obtain the closed loop transfer function:

$$\frac{r}{r_{sp}} = \frac{K_d K/T}{s + K/T(\alpha + K_d)}. \tag{11}$$

A feedback gain $K_d > -\alpha$ will stabilise this system, as also found in Neuffer and Owens (1991). With this stabilised inner loop, the outer loop will be designed.

4.1.2. Course controller

The linear transfer function from the required rate-of-turn to the course is a series connection of (4) and (11):

$$\frac{\chi}{r_{sp}} = \frac{(\tau_{z_1} s + 1)(\tau_{z_2} s + 1)}{s(\tau_p s + 1)} \frac{K_d K/T}{s + K/T(\alpha + K_d)}. \tag{12}$$

If we design our feedback controller to cancel the stable pole at τ_p and the stable zero τ_{z_1} and use a gain of K_p to close the loop:

$$C_{\chi,fb} : r_{sp} = K_p \frac{\tau_p s + 1}{\tau_{z_1} s + 1}(\chi_{sp} - \chi), \tag{13}$$

then we get the characteristic equation:

$$f(s) = s^2 + s\left(K/T(\alpha + K_d) + \tau_{z_2} K_p K_d K/T\right) + K_p K_d K/T. \tag{14}$$

The poles can be selected such that the system mimics a second order system with natural frequency ω_n and relative damping ζ if the gains are selected as:

$$K_d = \omega_n (T/K)(2\zeta - \tau_{z_2}\omega_n) - \alpha, \tag{15}$$

$$K_p = (T/K)(\omega_n^2/K_d). \tag{16}$$

The value of K_d should be larger than $-\alpha$ to stabilise the inner loop, which is always true when using this equation. We select $\omega_n = -1/\tau_{z_2}$, and in general we set $\zeta > 0.8$. Since we relate the bandwidth

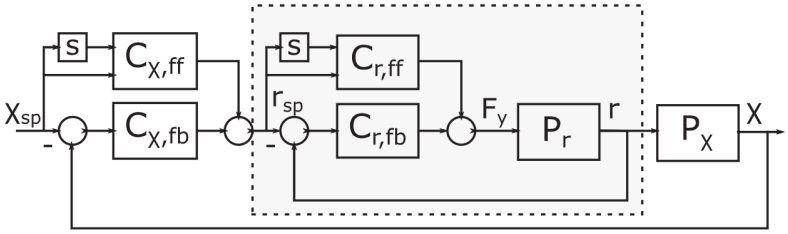

Figure 5. Control setup for the course control. The ship response from lateral force, F_y to rate-of-turn r is indicated by block P_r, (1). The ship response from rate-of-turn to course χ by the block P_χ (3). The controller for the rate-of-turn C_r contains a feedback (fb) and feed forward (ff) part. The inner loop is depicted in the gray box. The rate-of-turn setpoint is provided by controller of the outer loop C_χ. This controller calculates a rate-of-turn setpoint r_{sp} such that the course set point χ_{sp} is tracked. It consists again of a feedback and feed forward part. The 's' denotes a differentiation.

to the location of right-half-plane zero, we decrease the bandwidth for lower velocities. This is needed, as this zero poses a fundamental bound on the bandwidth (Skogestad and Postlethwaite 2007).

The feed forward controller is the inverse of the stable part of the transfer from the required rate to the course:

$$C_{\chi,\mathrm{ff}} : r_{\mathrm{sp}} = \frac{s(\tau_p s + 1)}{\tau_{z_1} s + 1} \chi_{\mathrm{sp}}. \tag{17}$$

Note that this transfer function is not proper, but we have access to the analytic time derivatives of the reference signal, so it can be implemented.

4.2. Speed controller

The linearised system of (5) is an open integrator. A single feedback gain is used as feedback controller. Integral action could be used, but this will only be advantageous for constant speeds, which will not

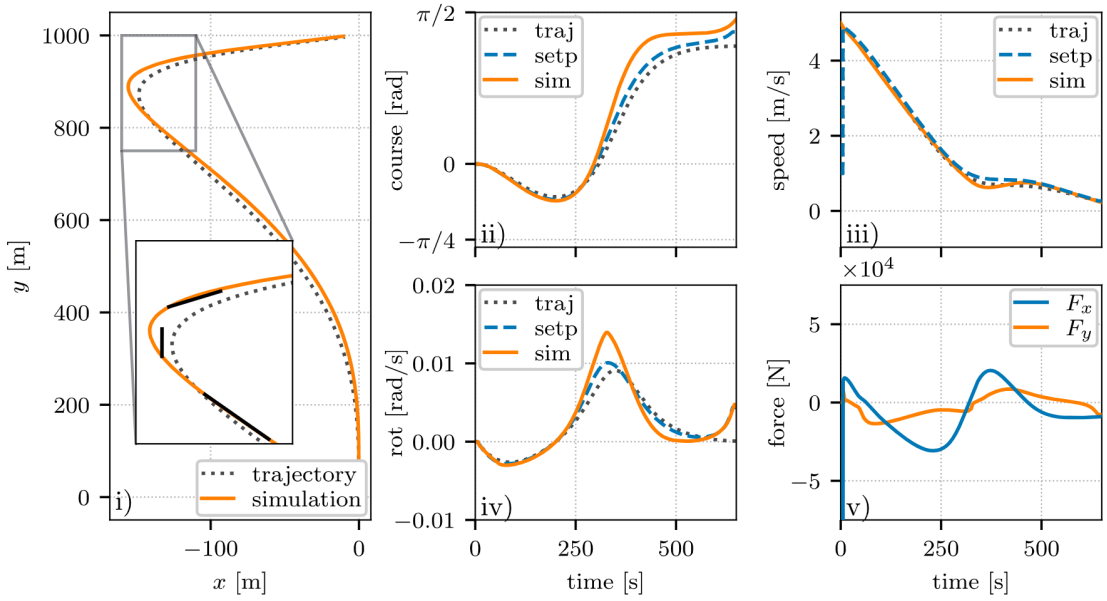

(a)

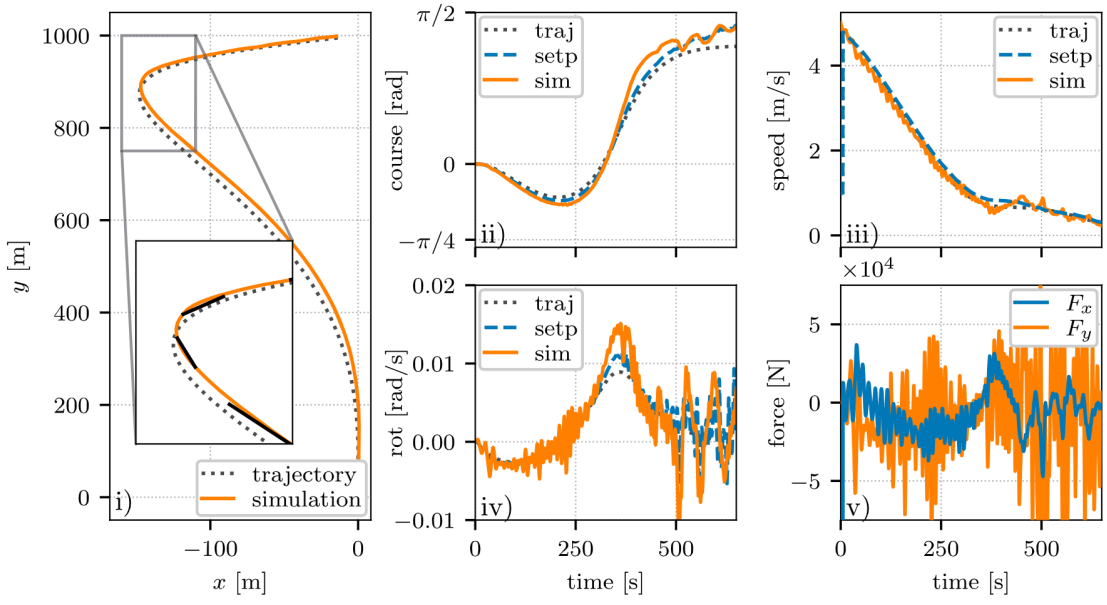

(b)

Figure 6. Simulation showing the approach to the dock of the underactuated feeder vessel. In subfigure (i) till (iv) the dotted gray lines indicate the original Bézier trajectory, the dashed blue lines show the setpoints calculated by the cb algorithm and the solid orange lines are the simulated responses. Subfigure (v) shows the calculated forces of the controller at the mean location of the azimuthing thrusters. The solid black lines in the insets are the velocity vector setpoints resulting from the cb guidance law (6). (a) simulation results without wind and wave disturbances and (b) simulation results with a wind speed of 5 m/s, and waves with $H_s = 0.5$ m from beam direction.

occur during the approaching phase. The forces due to the required acceleration and damping are fed forward. The equations for the controllers are:

$$C_{u,\text{fb}} : F_x = K(u_{\text{sp}} - u),$$
$$C_{u,\text{ff}} : F_x = (m - X_{\dot{u}})\dot{u}_{\text{sp}} - X_{u|u|}u_{\text{sp}}|u_{\text{sp}}|. \quad (18)$$

5. Results

The detailed numerical model (Section 2) was used to test the behaviour of the control scheme. The control forces were mapped to the coupled azimuthing thrusters, and their limits were respected in the simulation. The identified parameters were used in the feed forward controller. The bandwidth of the course feedback controller was scaled with the surge velocity, and it was capped at a maximum of $\omega_{\text{n}} = 0.2$ rad/s. In order to avoid overshoot, a relative damping of $\zeta = 1$ was used. The maximum velocity with which the vessel approaches the target position was used to select the value for the parameter $U_{\text{max}} = 0.25$ m/s. As argued before, this value should be lower than the speed at which the bow thrusters would become effective, and the controller would become fully actuated. The value $\Delta = 15$ m was found by increasing its value until a smooth motion to the target position was realised. The static feedback gain for the speed controller was set to $K = 10^5$ N/(m/s), which results in a closed loop bandwidth of $\omega = 0.03$ rad/s.

Results of the simulation are shown in Figure 6. The environmental forces (wind and waves) acting on the vessel are shown in Figure 7. Statistics for different wind disturbances are shown in Table 2. Figure 6(a) shows the results without any disturbances, while Figure 6(b) includes wind speed of 5 m/s and waves with a significant wave height $H_{\text{s}} = 0.5$ m/s, and a period of $T_{\text{p}} = 12$ sec in the direction of the dock. The waves hit the ship sideways when it was at the dock. The Bézier reference trajectory is shown by the dotted grey line in the figure.

Figure 6(a)(i) shows the vessel path as well as the reference path. The maximum tracking error, emphasised at the zoom-inset, is approximately 16 m. In this part of the trajectory there is a large curvature with a surge speed above 1.25 m/s, and the vessel is drifting significantly. Even though a feed forward controller was used to improve tracking behaviour, the differences in the detailed numerical model and our approximate control model result in tracking errors. In the final straight approach to the dock, these tracking errors are nullified by the feedback controller.

In the inset the black lines indicate the target velocities that stem from the CB algorithm. It shows that the required velocity direction is not only targeted to minimise the current cross track error, but it also incorporates the actual trajectory velocity.

The course and heading are depicted in Figure 6(a)(ii), while the rate-of-turn in shown in Figure 6(a)(iv). The dotted line shows the tangent of the Bézier curve, while the blue dashed line shows the output of the CB algorithm. These are close together, but there is a small difference in order to move the vessel in the direction of its target. The orange line is the *heading* of the simulated vessel. The heading will be different from the course, especially at higher rate-of-turns. This can be seen at $t \approx 300$ sec when comparing (ii) with (iv). At the end of the simulation the heading is moving away from the course, even with a required rate-of-turn of zero. This occurs at a low speed $u < 0.5$ m/s. The bandwidth of the course controller at this speed needs to be low due to the minimum phase behaviour, see Figure 3. If the CB algorithm tries to move the ship to the correct location, the ship will turn due to the location of the azimuthing thrusters. This is not problematic, as at these speeds the bow thrusters are effective and can counter the rotation.

Figure 6(a)(iii) shows the tracking of the speed. The maximum error found was found to be approximately 0.2 m/s, while this error decreases again when approaching the dock. The control forces are dominated by the forces that result from the feed forward controller, not shown here. Figure 6(a)(v) shows the requested forces. Around $t \approx 250$ sec the longitudinal and lateral forces change direction. The azimuthing thrusters can only turn at 12 degrees per second. The effects of this slow rotation can be observed at the zero-crossing.

Figure 6(b) shows the same signals but with wind and wave disturbances. The course realised is slightly changed due to the wind. A further increase in wind speed increases this effect. The effect of the waves is significant. They approach from the beam, and this introduces oscillations around the course. As the ship is course unstable, the gain acting on the rate-of-turn has to be rather large to stabilise the course, see Section 4.1.1. This results in large lateral forces as seen in Figure 6(b)(v). The azimuthing thrusters are not able to rotate fast enough to these force requirements. A notch-filter to selectively omit the wave frequencies can mitigate this problem (Marshfield 1991), among other filter options.

Finally, Table 2 provides some statistics on the tracking performance of the controller during the approach. A wind of 8.85 m/s was used in the simulations from different directions. The wind speed in the port of Mykonos is below this value for 70% of the time. No current and waves are used in these simulation. The smallest error at the end of the trajectory is found when the final approach of the ship is against the wind. The worst performance keeps the maximum deviation to the track smaller than half of the ship's length. At the end of the approaching phase, the DP system should bring the ship slowly to the dock.

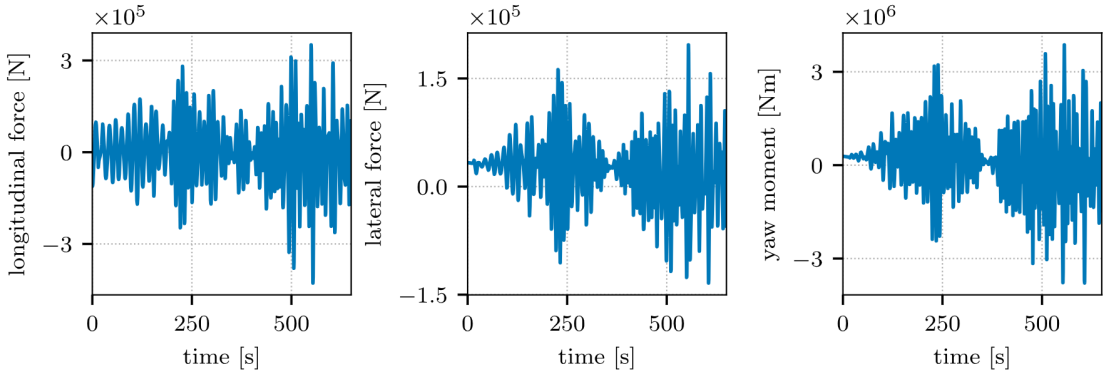

Figure 7. Environmental forces acting on the ship. The ship motions are provided in Figure 6(b).

Table 2. The distance to the Bézier curve for wind from different directions with a windspeed of 8.85 m/s.

direction	$\tilde{p}_{max}$ [m]	$\tilde{p}_{rms}$ [m]	$\tilde{p}_{bt}$ [m]	$\tilde{p}_{end}$ [m]	u_{end} [m/s]
no dist.	16.2	8.2	2.1	12.5	0.06
0°	17.3	12.8	16.4	23.8	0.10
45°	31.0	16.1	10.1	9.8	0.14
90°	32.6	15.5	9.5	8.5	0.14
135°	26.8	14.9	22.1	17.6	0.13
180°	31.5	12.2	31.6	23.0	0.13
225°	12.6	8.4	11.8	23.4	0.12
270°	22.2	9.7	22.4	20.2	0.10
315°	19.9	10.9	14.0	27.5	0.10

Note: The port of Mykonos has a wind speed below 8.85 m/s for 70% of the time. The columns indicate, respectively, maximum distance to the path, rms distance to the path, distance to the path when the bow thrusters become active at $u = 0.25$ m/s, and the distance to the path at the end of the trajectory. The right-most column shows the remaining velocity at the end of the phase. The first row is without disturbances.

6. Conclusions

In this study a controller to approach a dock was designed and tested for an underactuated course unstable feeder vessel. In order to do this, an available high fidelity model is simplified such that it could be used for control design. A smooth trajectory that brings the vessel from the current position and orientation close to the dock could be tracked with the controller. As the controller is designed as a cascade controller, intermediate signals have a clear interpretation.

The speed and course were independently controlled, although the speed was a parameter in the course keeping controller. There were deviations between the sailed track and the required track, even though a feed forward controller was used based on identified coefficients. This indicates that the control model is not perfect, and a feedback controller is not only needed to stabilise the course unstable system, but also to counter modelling inaccuracies.

At the end of the manoeuvre, at very low speeds, the ship is difficult to handle without bow thrusters. This is acceptable, as the bow thrusters are be effective in that speed range, and a dynamic positioning controller can bring the vessel slowly to the dock.

In the current work we have presented a linear controller that can bring the vessel close to a pose with near zero velocity. Future work needs to investigate realistic disturbances due to the quay and shallow water effects on the performance. A control design that can inherently cope with these disturbances, uncertainty and coupling between the degrees of freedom might be necessary. Furthermore, a full docking manoeuvre will be tested in our basins in the near future.

Disclosure statement

No potential conflict of interest was reported by the author(s).

Funding

MOSES project has received funding from the European Union's Horizon 2020 research & innovation programme under grant agreement No. 861678. Content reflects only the authors' view and the Agency is not responsible for any use that may be made of the information it contains.

ORCID

Bas J. de Kruif http://orcid.org/0000-0003-0086-0484

References

Ahmed Y, Hasegawa K. 2015. Consistently trained artificial neural network for automatic ship berthing control. TransNav Int J Mar Navig Saf Sea Transp. 9(3):417–426. http://www.transnav.eu/Article_Consistently_Trained_Artificial_Ahmed,35,600.html

Bitar G, Martinsen AB, Lekkas AM, Breivik M. 2020. Trajectory planning and control for automatic docking of ASVs with full-scale experiments. IFAC-PapersOnLine. 53(2):14488–14494. doi: 10.1016/j.ifacol.2020.12.1451

Breivik M. 2010. Topics in guided motion control of marine vehicles [dissertation]. Norwegian University of Science and Technology. https://www.researchgate.net/publication/215523092.

de Kruif BJ. 2022a. Applied trajectory generation to dock a feeder vessel. IFAC-PapersOnLine. 55(31):172–177. doi: 10.1016/j.ifacol.2022.10.427

de Kruif BJ. 2022b. Autonomous docking of a feeder vessel. In: International ship control systems symposium (iSCSS). Delft: The Netherlands.

Djouani K, Hamam Y. 1995. Minimum time-energy trajectory planning for automatic ship berthing. IEEE J Ocean Eng. 20(1):4–12. doi: 10.1109/48.380251

Fossen TI. 2021. Handbook of marine craft hydrodynamics and motion control. 2nd ed. Trondheim (Norway): John Wiley & Sons Ltd.

Fruzzetti C, Donnarumma S, Martelli M. 2022. Dynamic target chasing: parameters and performance indicators assessment. J Mar Sci Technol. 27(1):712–729. doi: 10.1007/s00773-021-00865-3

Kamermans M. 2022. A primer on Bézier curves. [accessed 2021-12-21]. https://pomax.github.io/bezierinfo/.

Li S, Liu J, Negenborn RR, Wu Q. 2020. Automatic docking for underactuated ships based on multi-objective nonlinear model predictive control. IEEE Access. 8:70044–70057. doi: 10.1109/Access.6287639

Liao Y, Jia Z, Zhang W, Jia Q, Li Y. 2019. Layered berthing method and experiment of unmanned surface vehicle based on multiple constraints analysis. Appl Ocean Res. 86(July 2018):47–60. doi: 10.1016/j.apor.2019.02.003

Liu X, Ren J, Wang H. 2020. Optimal energy trajectory planning and control for automatic ship berthing. In: 2020 39th Chinese control conference (CCC). jul. IEEE. p. 1420–1425. https://ieeexplore.ieee.org/document/9188805/.

MARIN. 2022. aNySIM XMF. [accessed 2022-05-24]. https://www.marin.nl/en/facilities-and-tools/software/anysim.

Marshfield WB. 1991. Submarine periscope-depth depth-keeping using an H-infinity controller together with sea-noise-reduction notch filters. Trans Inst Meas Control. 13(5):233–240. doi: 10.1177/014233129101300503

Martinsen AB, Lekkas AM, Gros S. 2019. Autonomous docking using direct optimal control. IFAC-PapersOnLine. 52(21):97–102. doi: 10.1016/j.ifacol.2019.12.290

Martinsen AB, Lekkas AM, Gros S. 2020. Combining system identification with reinforcement learning-based MPC. IFAC-PapersOnLine. 53:8130–8135. doi: 10.1016/j.ifacol.2020.12.2294

Mizuno N, Uchida Y, Okazaki T. 2015. Quasi real-time optimal control scheme for automatic berthing. IFAC-PapersOnLine. 48(16):305–312. doi: 10.1016/j.ifacol.2015.10.297

Moses. 2023. MOSES: automated vessels and supply chain optimisation for sustainable short sea shipping. [accessed 2023-03-20]. https://moses-h2020.eu/.

Neuffer D, Owens DH. 1991. Global stabilization of unstable ship dynamics using PD control Proceedings of the 30th IEEE Conference on Decision and Control.

Ohtsu K, Shoji K, Okazaki T. 1996. Minimum-time maneuvering of a ship, with wind disturbances. Control Eng Pract. 4(3):385–392. doi: 10.1016/0967-0661(96)00016-0

Okazaki T, Ohtsu K. 2008. A study on ship berthing support system – minimum time berthing control. In: 2008 IEEE international conference on systems, man and cybernetics. oct. IEEE. p. 1522–1527. http://ieeexplore.ieee.org/document/4811502/.

Piao Z, Guo C, Sun S. 2019. Research into the automatic berthing of underactuated unmanned ships under wind loads based on experiment and numerical analysis. J Mar Sci Eng. 7(9):300. doi: 10.3390/jmse7090300

Ravikumar L, Padhi R, Philip NK. 2020. Trajectory optimization for rendezvous and docking using nonlinear model predictive control. IFAC-PapersOnLine. 53(1):518–523. doi: 10.1016/j.ifacol.2020.06.087

Sawada R, Hirata K, Kitagawa Y, Saito E, Ueno M, Tanizawa K, Fukuto J. 2021. Path following algorithm application to automatic berthing control. J Mar Sci Technol. 26(2):541–554. doi: 10.1007/s00773-020-00758-x

Shneydor NA. 1998. Missile guidance and pursuit kinematics, dynamics and control. Oxford: Woodhead Publishing

Skejic R, Breivik M, Fossen TI, Faltinsen OM. 2009. Modeling and control of underway replenishment operations in calm water. IFAC Proc Vol. 42(18):78–85. doi: 10.3182/20090916-3-BR-3001.0022

Skogestad S, Postlethwaite I. 2007. Multivariable feedback control: analysis and design. Vol. 2. New York: Wiley

Tzeng CY, Lee SD, Ho YL, Lin WL. 2006. Autopilot design for track-keeping and berthing of a small boat. In: Conference proceedings – IEEE international conference on systems, man and cybernetics. Vol. 1. oct; Taipei, Taiwan: IEEE. p. 669–674. http://ieeexplore.ieee.org/document/4273909/.

van Daalen EFG, Iavicoli G, Cozijn H, de Kruif BJ. 2023. Simulation of a feeder on a port-to-port mission. In: Oceans 2023. Limerick, Ireland.

Yu Z, Bao X, Nonami K. 2008. Course keeping control of an autonomous boat using low cost sensors. J Syst Des Dyn. 2(1):389–400. http://www.jstage.jst.go.jp/article/jsdd/2/1/2_1_389/_article

Appendices

Appendix 1. Bézier curve

The target position is based on a cubic Bezier curve (Kamermans 2022):

$$\boldsymbol{p}_\mathrm{t}(h) = (1-h)^3\boldsymbol{p}_0 + 3(1-h)^2h\boldsymbol{p}_1 + 3(1-h)h^2\boldsymbol{p}_2 + h^3\boldsymbol{p}_3. \tag{A1}$$

With $0 \leq h \leq 1$ the path variable. The variables used are shown in Figure A1 with $\boldsymbol{p}_\mathrm{t} = [p_{\mathrm{t},x}, p_{\mathrm{t},y}]^T$ and $\boldsymbol{p}_i = [p_{i,x}, p_{i,y}]^T$. When we set $h = 0$ then this function evaluates to $\boldsymbol{p}_\mathrm{t}(0) = \boldsymbol{p}_0$, and at $h = 1$ we get $\boldsymbol{p}_\mathrm{t}(1) = \boldsymbol{p}_3$. The derivative with respect to h is calculated as:

$$\frac{\mathrm{d}\boldsymbol{p}_\mathrm{t}}{\mathrm{d}h}(h) = 3(1-h)^2(\boldsymbol{p}_1 - \boldsymbol{p}_0) + 6(1-h)h(\boldsymbol{p}_2 - \boldsymbol{p}_1) + 3h^2(\boldsymbol{p}_3 - \boldsymbol{p}_2). \tag{A2}$$

At $h = 0$ and $h = 1$ this evaluates to $\frac{\mathrm{d}\boldsymbol{p}_\mathrm{t}}{\mathrm{d}h}(0) = 3(\boldsymbol{p}_1 - \boldsymbol{p}_0)$ and $\frac{\mathrm{d}\boldsymbol{p}_\mathrm{t}}{\mathrm{d}h}(1) = 3(\boldsymbol{p}_3 - \boldsymbol{p}_2)$. So, the tangent at the start and the end are given by the vector to the adjacent control point. The path variable needs to become time-dependent to convert the path to a time-dependent trajectory. The target surge speed can then be calculated as:

$$u_\mathrm{t}(t) = \sqrt{\left(\frac{\mathrm{d}p_{\mathrm{t},x}}{\mathrm{d}t}\right)^2 + \left(\frac{\mathrm{d}p_{\mathrm{t},y}}{\mathrm{d}t}\right)^2} = \frac{\mathrm{d}h}{\mathrm{d}t}\sqrt{\left(\frac{\mathrm{d}p_{\mathrm{t},x}}{\mathrm{d}h}\right)^2 + \left(\frac{\mathrm{d}p_{\mathrm{t},y}}{\mathrm{d}h}\right)^2}. \tag{A3}$$

Note that the surge velocity is *defined* to be positive. Evaluating the target surge speed at $h = 0$ and $h = 1$ results in

$$u_0 = 3l_0\frac{\mathrm{d}h(0)}{\mathrm{d}t}, \quad u_\mathrm{f} = 3l_\mathrm{f}\frac{\mathrm{d}h(1)}{\mathrm{d}t}. \tag{A4}$$

As we want to end at zero speed, $u_\mathrm{f} = 0$ and we want to have l_f finite, we need $\frac{\mathrm{d}h(1)}{\mathrm{d}t} = 0$. The polynomial $h(t) = t/T(2 - t/T)$, among many others, achieves this. T is the duration of travelling the trajectory. The derivative at $t = 0$ evaluates to $\frac{\mathrm{d}h(0)}{\mathrm{d}t} = 2/T$. This can be related to the initial velocity:

$$u_0 = \frac{6l_0}{T} \rightarrow h = \frac{tu_0}{6l_0}\left(2 - \frac{tu_0}{6l_0}\right). \tag{A5}$$

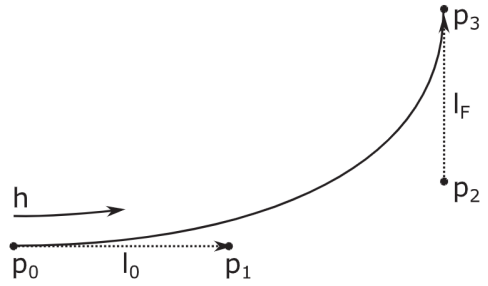

Figure A1. The principle variables of a cubic Bezier curve. p_i are the control points, and $0 \leq h \leq 1$ is the path variable.

Appendix 2. Setpoint derivatives

The time derivatives of the Bézier curve are found by using the chain rule:

$$\boldsymbol{v}_\mathrm{t} = \frac{\mathrm{d}\boldsymbol{p}_\mathrm{t}}{\mathrm{d}t} = \frac{\mathrm{d}\boldsymbol{p}}{\mathrm{d}h}\frac{\mathrm{d}h}{\mathrm{d}t} \tag{A6}$$

$$\frac{\mathrm{d}\boldsymbol{v}_\mathrm{t}}{\mathrm{d}t} = \frac{\mathrm{d}^2\boldsymbol{p}_\mathrm{t}}{\mathrm{d}t^2} = \frac{\mathrm{d}^2\boldsymbol{p}}{\mathrm{d}h^2}\left(\frac{\mathrm{d}h}{\mathrm{d}t}\right)^2 + \frac{\mathrm{d}\boldsymbol{p}}{\mathrm{d}h}\frac{\mathrm{d}^2h}{\mathrm{d}t^2} \tag{A7}$$

These derivatives contain the earth-fixed x- and y-component. The derivative of the setpoint surge speed to the vehicle controller, (7), is:

$$\frac{\mathrm{d}u_\mathrm{sp}}{\mathrm{d}t} = \frac{v_{\mathrm{sp},x}\frac{\mathrm{d}}{\mathrm{d}t}v_{\mathrm{sp},x} + v_{\mathrm{sp},y}\frac{\mathrm{d}}{\mathrm{d}t}v_{\mathrm{sp},y}}{u_\mathrm{sp}}, \tag{A8}$$

$\boldsymbol{v}_\mathrm{sp} = [v_{\mathrm{sp},x}, v_{\mathrm{sp},y}]^T$ is known from (6). The components of the acceleration are a summation of the target acceleration and acceleration to bring the vessel to the target:

$$\frac{\mathrm{d}\boldsymbol{v}_\mathrm{sp}}{\mathrm{d}t} = \frac{\mathrm{d}\boldsymbol{v}_\mathrm{t}}{\mathrm{d}t} + \frac{\mathrm{d}\boldsymbol{v}_\mathrm{a}}{\mathrm{d}t}. \tag{A9}$$

The first term on the right hand side follows from (A7). The second term is calculated as:

$$\frac{\mathrm{d}\boldsymbol{v}_a}{\mathrm{d}t} = \frac{\mathrm{d}\gamma}{\mathrm{d}t}\frac{\tilde{\boldsymbol{p}}}{||\tilde{\boldsymbol{p}}||} + \gamma\frac{\mathrm{d}}{\mathrm{d}t}\left(\frac{\tilde{\boldsymbol{p}}}{||\tilde{\boldsymbol{p}}||}\right), \tag{A10}$$

$$\frac{\mathrm{d}\gamma}{\mathrm{d}t} = U_\mathrm{max}\frac{\Delta^2(\tilde{p}_x\tilde{v}_x + \tilde{p}_y\tilde{v}_y)}{\left(\tilde{\boldsymbol{p}}^T\tilde{\boldsymbol{p}} + \Delta^2\right)^{\frac{3}{2}}\sqrt{\tilde{\boldsymbol{p}}^T\tilde{\boldsymbol{p}}}}, \tag{A11}$$

$$\frac{\mathrm{d}}{\mathrm{d}t}\left(\frac{\tilde{\boldsymbol{p}}}{||\tilde{\boldsymbol{p}}||}\right)_x = \frac{\left(-\tilde{p}_x\tilde{v}_x - \tilde{p}_y\tilde{v}_y\right)\tilde{p}_x}{\left(\tilde{\boldsymbol{p}}^T\tilde{\boldsymbol{p}}\right)^{\frac{3}{2}}} + \frac{\tilde{v}_x}{\sqrt{\tilde{\boldsymbol{p}}^T\tilde{\boldsymbol{p}}}}, \tag{A12}$$

$$\frac{\mathrm{d}}{\mathrm{d}t}\left(\frac{\tilde{\boldsymbol{p}}}{||\tilde{\boldsymbol{p}}||}\right)_y = \frac{\left(-\tilde{p}_x\tilde{v}_x - \tilde{p}_y\tilde{v}_y\right)\tilde{p}_y}{\left(\tilde{\boldsymbol{p}}^T\tilde{\boldsymbol{p}}\right)^{\frac{3}{2}}} + \frac{\tilde{v}_y}{\sqrt{\tilde{\boldsymbol{p}}^T\tilde{\boldsymbol{p}}}}, \tag{A13}$$

in which $\tilde{v}_x$ is the difference in the velocity between the target and the ship in the earth fixed x-coordinate. The same holds for the y-component. The time derivative of the course setpoint (7) is calculated as:

$$\frac{\mathrm{d}\chi_\mathrm{sp}}{\mathrm{d}t} = \frac{v_{\mathrm{sp},x}\frac{\mathrm{d}}{\mathrm{d}t}v_{\mathrm{sp},y} - v_{\mathrm{sp},y}\frac{\mathrm{d}}{\mathrm{d}t}v_{\mathrm{sp},x}}{u_\mathrm{sp}^2} \tag{A14}$$

Again, the velocity setpoint follows from (6). It's derivative is the addition of $\frac{\mathrm{d}\boldsymbol{v}_\mathrm{t}}{\mathrm{d}t}$ (A7) and $\frac{\mathrm{d}\boldsymbol{v}_\mathrm{a}}{\mathrm{d}t}$ (A10)–(A13).